TOPICAL REVIEW — Low-dimensional nanostructures and devices

Intercalation of metals and silicon at the interface of epitaxial graphene and its substrates*

Huang Li(黄 立)[a)b)], Xu Wen-Yan(徐文焱)[a)], Que Yan-De(阙炎德)[a)], Mao Jin-Hai(毛金海)[a)], Meng Lei(孟 蕾)[a)], Pan Li-Da(潘理达)[a)], Li Geng(李 更)[a)], Wang Ye-Liang(王业亮)[a)], Du Shi-Xuan(杜世萱)[a)], Liu Yun-Qi(刘云圻)[b)], and Gao Hong-Jun(高鸿钧)[a)†]

[a)] *Institute of Physics, Chinese Academy of Sciences, Beijing* 100190, *China*
[b)] *Institute of Chemistry, Chinese Academy of Sciences, Beijing* 100190, *China*

(Received 30 July 2013)

Intercalations of metals and silicon between epitaxial graphene and its substrates are reviewed. For metal intercalation, seven different metals have been successfully intercalated at the interface of graphene/Ru(0001) and form different intercalated structures. Meanwhile, graphene maintains its original high quality after the intercalation and shows features of weakened interaction with the substrate. For silicon intercalation, two systems, graphene on Ru(0001) and on Ir(111), have been investigated. In both cases, graphene preserves its high quality and regains its original superlative properties after the silicon intercalation. More importantly, we demonstrate that thicker silicon layers can be intercalated at the interface, which allows the atomic control of the distance between graphene and the metal substrates. These results show the great potential of the intercalation method as a non-damaging approach to decouple epitaxial graphene from its substrates and even form a dielectric layer for future electronic applications.

Keywords: graphene, metal intercalation, silicon intercalation, scanning tunneling microscopy

PACS: 68.65.Pq, 85.30.–z, 68.37.Ef **DOI:** 10.1088/1674-1056/22/9/096803

1. Introduction

Graphene, which was first exfoliated from graphite in 2004,[1] attracts increasing attention due to its unique structure and outstanding electronic, magnetic, and optical properties.[2–4] In the past few years, tremendous efforts have been made to fabricate large-area uniform graphene layers with low defect density, a material which is crucial for massive applications in future devices.[5–8] Epitaxial graphene on a single crystalline metal substrate,[7–15] especially on Ru(0001), is high quality and large in area, but has a strong interaction with the substrate, which hybridizes graphene's C π bond and disrupts its unique electronic properties. The previous work showed that this interaction can be effectively weakened via intercalating a layer of another element, such as Au,[16–18] Ag,[19,20] Cu,[21] and oxygen,[22,23] between the epitaxial graphene and its substrate, which makes the graphene regain its linear energy band dispersion or even open up a band gap around the Dirac point.[18] By using angle-resolved photoemission spectroscopy (ARPES) and electron-energy-loss spectroscopy (EELS), researchers found stiffening of graphite-derived phonon modes after intercalation, indicating that the intercalated layer effectively decouples epitaxial graphene from the substrate, making it behave more like a freestanding one.[16] Meanwhile, Premlal *et al.*[24] studied gold intercalation in graphene/SiC(0001) by scanning tunneling microscopy (STM) and scanning tunneling spectroscopy (STS), and found that different intercalated structures have different impacts on the electronic structure of graphene. These experimental results elucidate the great potential of intercalation to decouple epitaxial graphene from the substrate, and also indicate the crucial abilities of different intercalated structures for tuning graphene's electronic properties.

In this paper, we review demonstrations of the intercalations of two kinds of elements in epitaxial graphene/Ru(0001) or graphene/Ir(111). The first kind of elements is metals, including noble metals Pt, Pd, and Au, magnetic metals Ni and Co, the IIIA group metal In, and the rare earth metal Ce.[25] The other kind is semiconductor silicon.[26,27] The results reveal that the intercalation of any of the above elements through epitaxial graphene is a non-damaging approach. By metal intercalations, we obtain different intercalated structures for these metals. By silicon intercalation, we successfully form a layer of intercalated silicon, which not only blocks the interaction between graphene and its substrate, but also acts as a dielectric layer for future electronic applications. Through these findings, we are able to make use of the intercalation to tailor the electronic structure of graphene and integrate graphene into Si technology to harvest the best qualities that these materials could offer.

*Project supported by the National Basic Research Program of China (Grant Nos. 2013CBA01600, 2011CB932700, 2009CB929103, and 2010CB923004), the National Natural Science Foundation of China, and the Chinese Acedemy of Sciences.

†Corresponding author. E-mail: hjgao@iphy.ac.cn

2. Metal intercalations on graphene/Ru(0001)

In this part, we show STM studies of seven different metals, Pt, Pd, Ni, Co, Au, In, and Ce, intercalated at the interface of graphene/Ru(0001). As the previous work revealed, different intercalated structures may have different influences on the electronic structure of graphene.[24] We divide the seven metals into two categories according to the structures, specifically whether graphene still exhibits the same Moiré pattern on the top of the intercalated structure as it does when directly interfaced with Ru(0001).

The first category includes noble metals Pt, Pd and magnetic metals Ni, Co. These metals can be intercalated between graphene and Ru(0001) after annealing at 800 K. As shown in Figs. 1(a)–1(d), these intercalated structures are small islands in a symmetric triangular shape, with the edges along the same symmetric directions as the graphene Moiré pattern. The heights of these intercalated islands for Pt, Pd, Ni, and Co are 2.88 Å, 2.70 Å, 2.50 Å, and 3.00 Å, respectively, which are similar to or even smaller than the step height in a close packed crystal surface, indicating that the islands are only composed of a single atomic layer. On the top of these intercalated islands, graphene keeps the same Moiré pattern as on Ru(0001). Since the Moiré pattern is formed due to a lattice mismatch between graphene and the underlying substance, this unchanged Moiré structure implies that the lattices of the intercalated islands for these four metals have the same close packed hexagonal structure as that of Ru(0001).

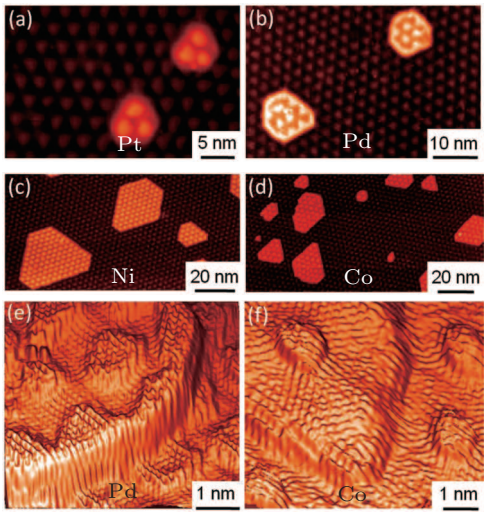

Fig. 1. STM topographic images: (a) Pt, (b) Pd, (c) Ni, and (d) Co intercalation structures in graphene/Ru(0001) after annealing at 800 K. (e) and (f) Atomic resolution images of graphene on a Pd-intercalated island and a Co-intercalated island, respectively. Scanning parameters are (a) −1.42 V, 0.13 nA; (b) −2.19 V, 0.11 nA; (c) −1.27 V, 0.13 nA; (d) −1.47 V, 0.13 nA; (e) −0.13 V, 2.12 nA; (f) −0.21 V, 1.97 nA.[25]

Although these islands have the same lattice parameters, they still differ in appearance. For instance, the edges of the Pd intercalated islands bulge to the same height as the Moiré atop region, which is very special among the four metals; and the mean sizes of the islands also differ. Pt tends to form small islands covering only two or three Moiré unit cells, while Ni prefers to form large islands that can spread across several hundreds of square nanometers. The conditions of the graphene layers on the top of the intercalated islands are shown by 3D STM images with atomic resolution in Figs. 1(e) and 1(f), in which the lattice of graphene is perfect with no additional defects and continuous across the edges of the intercalated islands, indicating that the intercalation process does no damage to the graphene.

The second category includes Au, In, and Ce, on which graphene has different corrugations from the Moiré pattern on Ru(0001), as illustrated in Fig. 2. In Figs. 2(a) and 2(c), Au and In intercalate between graphene and Ru(0001) after annealing at 500 K. The intercalated islands are much larger and scattered less densely than the ones in Fig. 1. For the Au-intercalated islands, the majority of the surface is flat with a height about 2.78 Å, which equals to the single step height of Au(111). In the case of In, the intercalated islands show varying heights ranging from monolayer to multi-layer. On the top of either of these metals, the graphene is very flat, indicating that the intercalated Au or In atoms do not grow with the same lattice as Ru(0001), but may be randomly arranged or reconstructed in some manner. For example, In atoms form a hexagonal reconstruction with a period of 4.80 Å, as shown in the inset of Fig. 2(c). The atomic resolution images in Figs. 2(b) and 2(d) show that the graphene lattice is perfect and continuous, both on the top of and at the edge of the islands, confirming that the intercalation does no harm to the quality of the graphene layer. Moreover, compared with the hexagonal lattice in the area with no intercalation, the graphene on the top of the intercalated islands displays a symmetric honeycomb lattice, which means that the strong interaction between graphene and the substrate has been blocked[28] and the graphene is more nearly freestanding after the intercalation, this is in agreement with the previous work.[16–18]

The intercalation of rare earth metal Ce is quite different from the metals mentioned above. Instead of annealing to 500 K or 800 K, the Ce intercalation happens at room temperature (RT) directly upon deposition on graphene/Ru(0001). Furthermore, a very special structure is formed when the Ce coverage is lower than 0.1 ML. As shown in Fig. 2(e), Ce atoms selectively intercalate from the atop and fcc regions of the Moiré structure. After intercalation, the atop and fcc regions of the graphene Moiré pattern have almost the same height and the hcp regions are left as indented holes, just like the geometry of h-BN "nanomesh".[29] This result demonstrates that the intercalation has a great potential to form interesting structures that can influence the geometry of graphene.

Meanwhile, the atomic resolution image of this graphene nanomesh (Fig. 2(f)) shows a perfect lattice without any defects, confirming again that the intercalation of Ce is a non-damaging process for graphene.

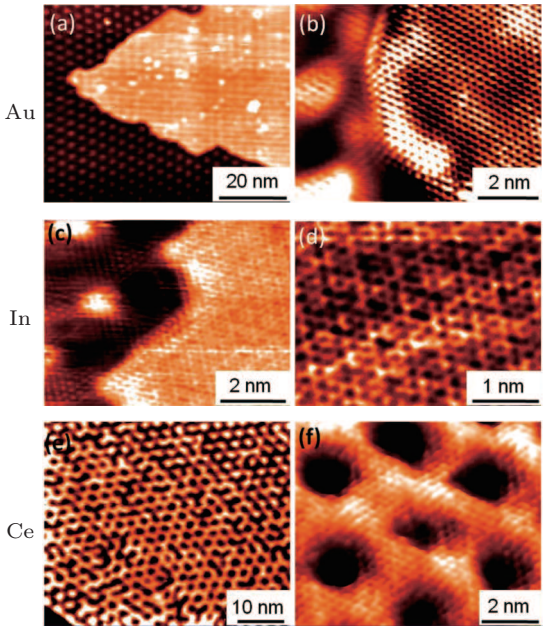

Fig. 2. STM topographic images. (a) Au-intercalated structure after annealing at 500 K. (b) Atomic resolution image across an edge of the Au-intercalated film. Graphene shows a honeycomb lattice on the top of the intercalated film. (c) Indium intercalated at 500 K with atomic resolution of on-top graphene. (d) Zoom-in image of honeycomb graphene lattice on the top of the In-intercalated film. (e) Nanomesh structure arising from low coverage Ce-intercalation at RT. (f) Atomic resolution image of graphene on the nanomesh structure in panel (e). Scanning parameters are (a) −2.96 V, 0.05 nA; (b) -0.10 V, 0.40 nA; (c) and (d) −0.04 V, 1.34 nA; (e) −0.61 V, 0.12 nA; (f) 0.03 V, 1.16 nA.[25]

For all the seven metals we've tried, graphene's high quality is always undisturbed during the intercalation process. Since additional defects may introduce unfavorable impacts on graphene, the non-damaging metal intercalation method demonstrated here might be a comparatively easy and harmless way to tune the electronic properties of epitaxial graphene.

3. Silicon intercalation in graphene/Ru(0001)

Having discussed metal intercalations, we next focus on silicon intercalation, which might provide a route for fabricating future graphene devices. In the following two parts, experiments with silicon intercalation in graphene/Ru(0001) and graphene/Ir(111) are introduced, and both show that silicon intercalation is a non-damaging process that can effectively block the interaction with the substrate and restore the graphene's superlative properties.

For silicon intercalation in graphene/Ru(0001), the experimental details are as follows. The Ru(0001) surface was prepared by Ar^+ sputtering and annealing to 1100 K, then exposed to oxygen at 1500 K to remove residual carbon, and then flashing to 1800 K to remove oxide. High quality graphene was prepared by thermal decomposition of ethylene on metal substrates at high temperature. The silicon was evaporated to the graphene surface, and then the sample was annealed at 800 K for 10 min. After cooling, we obtained STM/STS images/data in an ultrahigh vacuum (UHV) system equipped with an Omicron UHV-LT-STM at the temperature of 5 K. The chamber was also equipped with low energy electron diffraction (LEED) and Auger electron spectroscopy (AES) to monitor the quality of the graphene. STS was measured with a lock-in technique by applying a small modulation signal, AC 7 mV·rms at 730 Hz, to the tunneling voltage. The angle resolved electron photoemission spectroscopy (ARPES) measurements were carried out using our lab system equipped with a Scienta R4000 analyzer and a VUV5000UV source which gives the photon energy of Helium I at $h\nu = 21.218$ eV. The overall energy resolution was 10 meV and the angular resolution was 0.3°. The measurement was performed at 20 K in vacuum with a base pressure better than 5×10^{-11} Torr.

First, a highly ordered, centimeter-scale (0.8 cm in diameter), and continuous monolayer graphene of high quality on Ru(0001)[8] was prepared for the Si layer intercalation. The procedure for silicon-layer intercalation approach (SIA) is as follows: (i) growth of monolayer graphene on Ru(0001) (Fig. 3(a)); (ii) deposition of silicon on the surface of graphene (Fig. 3(b)); (iii) annealing the deposited Si and formation of the Si layer between the graphene and Ru (Fig. 3(c)). STM was used to image the surface of the sample at each of the three stages. For reference, the G/Ru(0001) surface structure is provided, showing the Moiré patterns that characterize the interaction between the Ru and graphene lattices (Fig. 3(d)). After Si deposition on the graphene/Ru(0001), Si clusters can be seen on the surface of the sample (Fig. 3(e)). After annealing at 800K, the Si deposited clusters disappeared and the sample became uniform and atomically flat (Fig. 3(f)).

The structural decoupling of the graphene from the Ru surface can be seen by the degree of flatness of the honeycomb lattice as compared with graphene grown directly on Ru(0001). The strong surface corrugation of graphene on Ru(0001) disappears after the Si intercalation, as shown in Fig. 3(g). Further zooming of the STM images shows clearly the honeycomb lattice of the monolayer graphene (Figs. 3(h) and 3(i)). DFT calculations of the interaction between the Si layer and the Ru(0001) surface reveal that it is very weak with a spacing of 3 Å between graphene and the silicon layer on Ru(0001). This structural decoupling leads to the high resolution STM images of the epitaxial graphene after the Si intercalation.

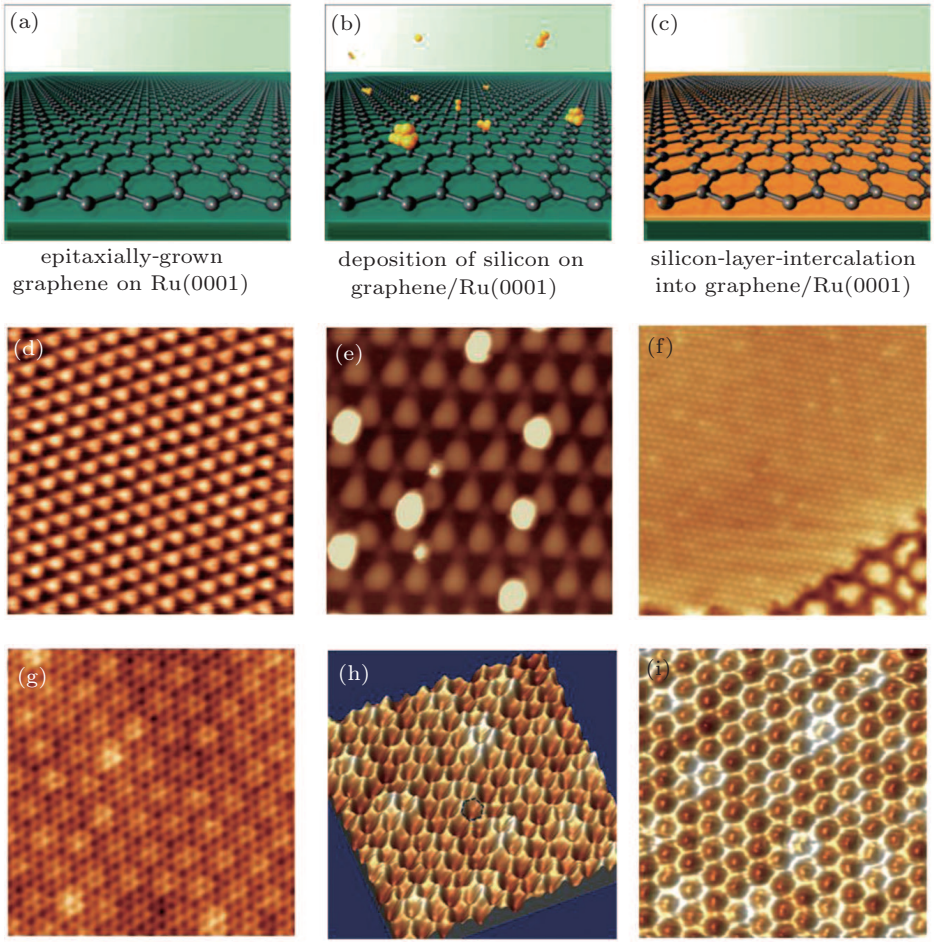

Fig. 3. SIA on Ru(0001). (a)–(c) Schematic diagrams of the silicon intercalation process: (a) graphene formation on Ru(0001); (b) Si deposition on graphene/Ru(0001); (c) annealing and Si layer intercalation. (d) STM image of graphene on Ru(0001), showing the ordered Moiré pattern, 40 nm × 40 nm, 0.1 nA, −3.0 V. (e) Silicon deposition on the graphene, 20 nm × 20 nm, 0.2 nA, −2.0 V. (f) After annealing, the Si intercalation between graphene and Ru(0001), 25 nm × 25 nm, 0.1 nA, −3.0 V. (g) Zoom-in STM image of G/Si/Ru, 6 nm × 6 nm, 0.1 nA, −1.0 V. (h), (i) 3D STM images of the G/Si/Ru surface, 3 nm × 3 nm, 0.2 nA, −1.0 V.[26]

In Fig. 4(a) ARPES measurements show that the conduction (π^*) and valence (π) bands cross at the Dirac point (E_D) at the K point of the hexagonal Brillouin zone, with a linear dispersion over a large energy range. The Dirac point is below the Fermi energy E_F by 0.26 eV, and the measured Fermi velocity (the slope of the cones in the Γ–K direction) is 0.95×10^6 m/s, that is, of the same magnitude as the Fermi velocity of graphene on SiO_2. This result implies a charge doping of about 2.7×10^{-3} electrons per unit cell, i.e., 5.1×10^{12} cm^{-2}. From constant energy maps of the states at E_F, E_D, and E_F −0.8 eV (Figs. 4(b)–4(d)), we can see the hole and electron pockets. The equal energy contours in the maps which correspond to the cone structure near the E_D are similar to the ARPES measurements of graphene epitaxially grown on SiC.[30,31] Another feature of the Si-intercalated graphene is that there is no replica around the Dirac point in the constant energy mapping, this is a phenomenon induced by the Moiré pattern and observed in graphene on either SiC(0001) or Ir(111). The absence of this feature may indicate that the SIG is more uniform and more like intrinsic graphene than graphene on a SiC or Ir surface. Thus, graphene on the G/Si/Ru structure is decoupled from its substrate and is not subject to any significant potential that would affect the spectral properties of the Dirac quasiparticles.

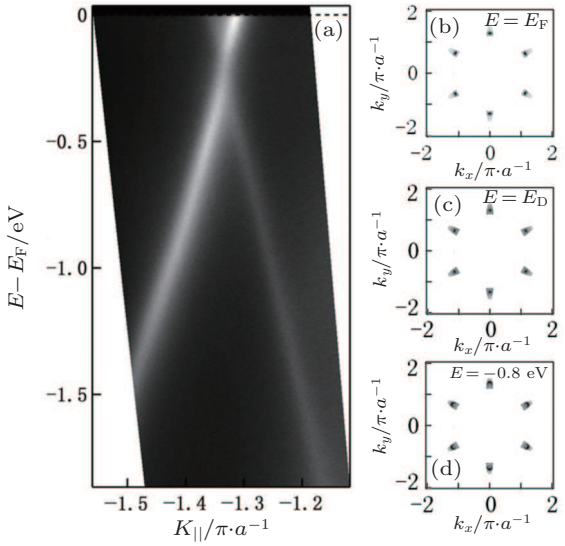

Fig. 4. ARPES on G/Si/Ru. (a) Electronic structure of the silicon-intercalated graphene along the Γ–K direction. (b)–(d) Constant energy maps at E_F, E_D, and $E_F - 0.8$ eV.[26]

Although impurities are usually considered to be a nuisance due to their deleterious effects on the electronic transport, they can also reveal important features of the electronic properties. We have selected a few samples in which we can find defects (such as a vacancy) that can be used as a probe of the electronic states of our samples. An STM image of G/Si/Ru containing a local defect is shown in Fig. 5(a). It shows the superstructure around the defect, which is assigned to the inter-valley scattering of the delocalized π electrons by the defect.[32] The fast Fourier transform (FFT) of the large area STM image with the same kind of defect is shown in Fig. 5(b) with the (1×1) and the R3 spots, corresponding to the superstructure. The same quantum interference patterns have been found in bilayer graphene directly on Ru(0001) and graphene on SiC(0001) surface. They are absent in monolayer graphene grown on a Ru(0001) surface and in the buffer layer of SiC(0001) where the π band is strongly perturbed.[6] Such interference patterns are fingerprints of the π states close to the Fermi level.[33] In the upright corner of Fig. 5(b) we show one of the R3 spots in the FFT image. The fine structure in these measurements agrees well with the theoretical predictions for the inter-valley scattering of chiral Dirac fermions.[34] This quantum interference at the atomic resolution demonstrates that the metallic states of the graphene in this G/Si/Ru structure are essentially decoupled from the underlying electronic states in the silicon on Ru(0001).

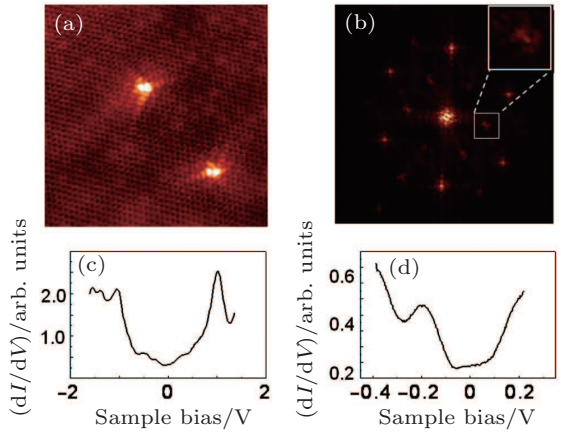

Fig. 5. Silicon-intercalated graphene. (a) STM image of the point defect on G/Si/Ru , 10 nm $\times$ 10 nm, 0.3 nA, -0.8 V. (b) FFT of the G/Si/Ru STM image at a low voltage, 2 mV, 0.3 nA. The zoomed-in FFT images show details of the inter-valley scattering spot. Each spot due to the inter-valley scattering is separated into two parts along the Γ–K direction. The $\mathrm{d}I/\mathrm{d}V$ at different bias scales: (c) $I = 0.3$ nA, $V = 1.5$ V; (d) $I = 0.3$ nA, $V = 0.4$ V.[26]

To investigate the electronic properties of G/Si/Ru, local tunneling conductance, $\mathrm{d}I/\mathrm{d}V$, was measured over the entire area. The typical profile of LDOS for graphene was observed at a low bias (Fig. 5(c)). Similar to graphene on SiO_2, the spectrum also shows a gap-like feature centered at the Fermi level and a local minimum at $V_D = -260$ mV (Fig. 5(d)). This gap-like feature can be interpreted as a suppression of electronic tunneling to graphene states near the Fermi energy and a simultaneous enhancement of electronic tunneling at higher energies due to a phonon-mediated inelastic channel.[34] The minimum at -0.26 V is associated with the Dirac point that is shifted to the electron doping side (the sample is slightly n-doped), which is in agreement with the ARPES experiments. Both the STS and the FFT-STM show a decoupling between graphene electrons and the substrate, which is due to the Si intercalation.

In order to investigate the intercalation of thicker Si layers between graphene and Ru(0001), we deposited more Si on the top of the already-formed monolayer-silicon intercalated graphene (G/1-Si/Ru) and then annealed the sample again. As shown in Fig. 6(a), STM images show the boundary of the bilayer Si intercalated graphene (G/2-Si/Ru) on the left and G/1-Si/Ru on the right sides of the figure. We can see that the height difference is around 0.3 nm, consistent with the thickness of an added Si monolayer. Figures 6(b) and 6(c) show high resolution images of graphene lattice on the G/2-Si/Ru. It can be seen that the graphene has become uniform and much flatter than that formed on the G/1-Si/Ru, indicating an even weaker interaction with the substrate. This result opens the doors for the atomic control of the distance between graphene and a metal gate (in this case Ru) by creating a G/N-Si/Ru structure (N is the number of Si layers), which would be very important for future applications.

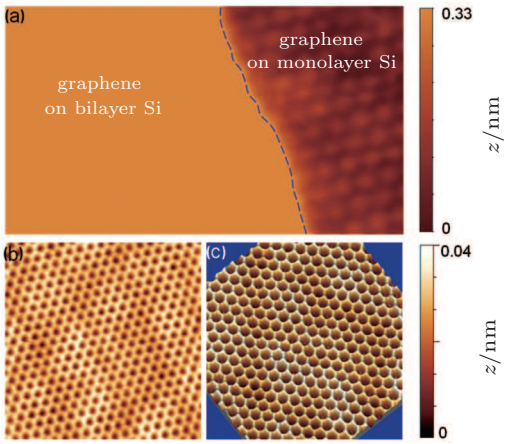

Fig. 6. STM images of G/2-Si/Ru. (a) In G/1-Si/Ru region, the Moiré pattern can be observed, 12 nm $\times$ 7 nm, 0.1 nA, -3.0 V. (b) and (c) High resolution STM images at the G/2-Si/Ru region, clearly showing each of the carbon atoms in the graphene lattice, 4.5 nm $\times$ 4.5 nm, 0.3 nA, -1.0 V.[26]

The results discussed above show that intercalation of Si layers at the interface of graphene and Ru maintains the graphene lattice intact and electronically decouples the graphene from the metal. Moreover, it is possible to intercalate thicker layers of Si, allowing for the atomic control of the distance between graphene and the metal substrate, opening doors for controllable high doping experiments with no need

for chemical doping. This technique is not exclusive to Ru, but can also be used on many other metal substrates that catalyze for graphene production, such as Ni, Ir, Cu, and Pt.

4. Silicon intercalation in graphene/Ir(111)

In this section, we will focus on silicon intercalation experiment in graphene/Ir(111). Graphene was fabricated by chemical decomposition of ethylene on an Ir(111) surface. Then silicon was deposited on the graphene/Ir(111) sample and annealed at 800 K, whereupon a distinct superstructure emerged and was characterized by LEED and STM, which was confirmed to have arisen due to the silicon intercalation. Further investigations of the electronic properties of the system were done by $\mathrm{d}I/\mathrm{d}V$ measurements and Raman spectroscopy on both graphene/Ir and graphene/Si/Ir, confirming that the silicon intercalation does successfully decouple the interaction between graphene and the Ir substrate.

The quality of graphene was first identified by the LEED pattern macroscopically. In Fig. 7(a), the inner six spots and the outer six spots, indicated by the dashed-line and solid-line arrows, can be easily distinguished and assigned to the Ir(111) lattice and the graphene adlayer, respectively. The additional satellite spots can be ascribed to the Moiré superstructure of graphene and are caused by the mismatch between graphene and the Ir substrate. Such an LEED pattern confirms that graphene has been epitaxially grown on the Ir(111) surface. Moreover, no rotational spots are found in Fig. 7(a) besides the six spots from graphene, which indicates that the graphene has only one orientation with respect to the Ir(111) substrate in our sample and that grapheme $[11\bar{2}0]$ is parallel to Ir $[1\bar{1}0]$.[35]

Figure 7(b) shows a typical STM image of this sample. A well ordered Moiré superstructure of graphene with a periodicity of about 2.5 nm is visible. The inset of Fig. 7(b) illustrates the atomic resolution of the graphene adlayer. The superimposed model depicts more clearly the honeycomb lattice of the carbon adlayer. Furthermore, the alignment of the honeycomb structure is almost parallel to Ir $[1\bar{1}0]$, which is consistent with the direction observed in the LEED pattern in Fig. 7(a). Therefore, considering the STM images together with the LEED pattern, we can confirm that a large scale graphene with a consistent orientation has been fabricated on the Ir(111) surface.

After the preparation of graphene, silicon was deposited onto the graphene/Ir(111) sample and then annealed to 800 K, which gave rise to a new superstructure, as shown in Fig. 7(c). This pattern is totally different from that in Fig. 7(a). In addition to the diffraction spots from Ir(111) and the graphene adlayer, a group of new spots appear within the circle of Ir(111) diffraction spots. These spots indicate the formation of another well ordered structure. We speculated at first that these spots are caused by silicon. In order to confirm this, we further used STM to observe the annealed sample, and found that the silicon clusters are no longer visible on the sample surface, instead, some distinct domains with locally ordered superstructures appear as shown in Fig. 7(d). The periodicity of this well ordered superstructure is about 1.2 nm, much smaller than the period of the graphene Moiré superlattice (2.5 nm). This superstructure is due to the intercalated silicon, as we will discuss later.

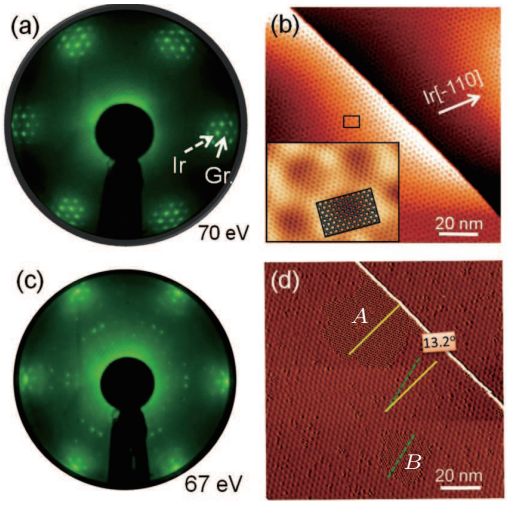

Fig. 7. LEED patterns and STM images of graphene on Ir(111) before and after silicon intercalation. (a) Before intercalation, the inner six spots and the outer six spots, indicated by the dashed-line and solid-line arrows, are from Ir(111) and the graphene adlayer, respectively. (b) Large-scale image ($V = -1.54$ V, $I = 0.05$ nA) shows a well ordered graphene adlayer with a Moiré superstructure of 2.5 nm. Inset is a zoomed-in image with atomic resolution inside a model superimposed on graphene indicating its orientation. (c) After silicon intercalation, a group of new spots appear within the circle of Ir(111) diffraction spots. (d) STM image ($V = -0.38$ V, $I = 0.13$ nA) showing two distinct ordered domains (marked as A and B) with a periodicity of 1.2 nm. Images (a) and (c) are obtained at 70 eV and 67 eV, respectively.[27]

It is worth noting that two small domains in Fig. 7(d) have different orientations. The orientation of region A is denoted by a solid line; region B has another orientation, which is denoted by a dashed line. The angle between these two orientations is about 13.2°. Based on the above analysis of the LEED pattern and STM images, this silicon-induced superstructure can be determined to be a $(\sqrt{19} \times \sqrt{19})$R23.41° Moiré superstructure. This superstructure includes two symmetrical orientations that are consistent with those of regions A and B. In addition, regions like region A are located at the step edges and regions like region B are located within the graphene adlayer. The locations indicate that the intercalation occurs both at the terrace and the step edges, suggesting that silicon intercalation starts both at the step edges and on the terraces.

We further expound the arrangement of the graphene adlayer and the intercalated Si layer. Figure 8(a) shows the domain boundary, denoted by the black dashed line, between a graphene/Ir area (with a periodicity of 2.5 nm) in the lower right and a silicon-intercalated graphene/Si/Ir area (periodicity 1.2 nm) in the upper left. It is easy to see several key

features in the intercalated area: graphene honeycomb lattice, $(\sqrt{19}\times\sqrt{19})$R23.41° superstructure, and even the silicon lattice underneath the graphene. The corresponding fast Fourier transform pattern (Fig. 8(b)) reveals the information more clearly. The pattern can be described as four distinct circles of spots, each including six spots with a hexagonal symmetry. In more detail, the innermost circle is associated with the 2.5 nm Moiré pattern caused by the mismatch between graphene and the Ir(111) lattice; the second circle arises from the $(\sqrt{19}\times\sqrt{19})$R23.41° Moiré superlattice induced by silicon intercalation; the third, larger one indicates a superstructure with a much smaller periodicity of about 0.44 nm, which we suppose to be the periodicity of the silicon structure formed underneath the graphene; and the outermost circle of spots is obviously from the lattice of graphene, which has the smallest periodicity 0.25 nm.

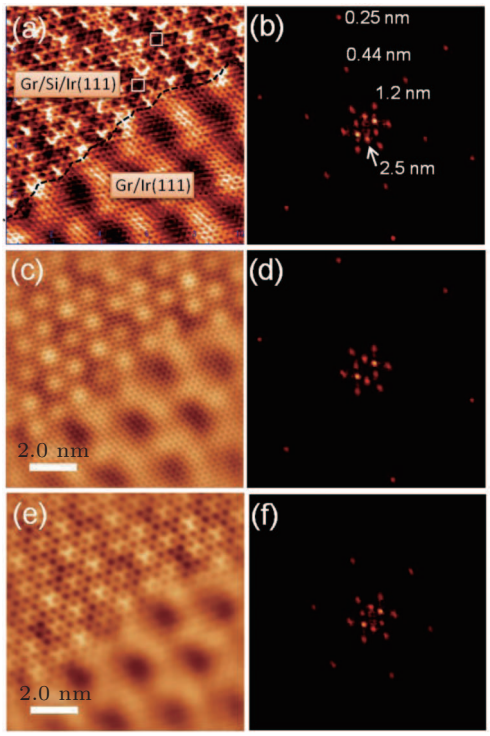

Fig. 8. Close-up STM images and corresponding FFT patterns at the domain boundary. (a) Atomically resolved image (10 nm × 10 nm, $V = -0.05$ V, and $I = 0.6$ nA) of graphene on Ir(111) with silicon-intercalated area on the upper-left region. (b) FFT pattern with four groups of spots with hexagonal symmetry, revealing four superstructures with different periodicities of 2.5 nm, 1.2 nm, 0.44 nm, and 0.25 nm from inner to outmost circles. Omitting the information of the superstructure with a periodicity of 0.44 nm and 0.25 nm, as seen in panels (d) and (f); the corresponding STM images are shown in panels (c) and (e). We can see that the topmost graphene layer (2.5 nm lattice) is intact and continuous in panel (c), and the underlying silicon layer (1.2 nm lattice) has a honeycomb structure in the upper-left region in panel (e).[27]

In Fig. 8(a), some dark sites (highlighted by the solid rectangles) are visible in the area of graphene/Si/Ir. There are three plausible explanations for these dark sites. First, the carbon atoms are missing from these sites.[32] Second, the atoms in the dark area are lower than other atoms in the surface geometry. Third, the local density of states at the dark site is less dense than that at other sites. Upon removing the third large circle of spots (0.44 nm in periodicity) from the FFT pattern by a high-pass treatment (see Fig. 8(d)), we get an image which nicely reveals the honeycomb lattice of the topmost graphene layer, as shown in Fig. 8(c). We see no sign of defects in this topmost lattice, so the first proposed explanation, missing carbon atoms, is ruled out. Since the applied bias voltage ($V_s = -0.05$ V) of this image is very close to the Fermi level, the image can be interpreted approximately as a $\mathrm{d}I/\mathrm{d}V$ mapping. Thus, we think that the darkness of certain sites in the STM image may be due to the relatively low LDOS at those sites, which is caused by the underlying silicon layer. Therefore, we conclude that the graphene lattice on our sample is still continuous and intact after the silicon intercalation.

Next we try to understand the ordered silicon layer beneath the graphene. As discussed above, the spots in the third large circle of the FFT pattern in Fig. 8(b) indicate an ordered superstructure of silicon with a periodicity of 0.44 nm. In order to get a clearer picture of this silicon structure, we eliminate the information of the topmost graphene honeycomb (0.25 nm in periodicity) from the FFT pattern, as depicted in Fig. 8(f). The corresponding STM image in Fig. 8(e) reveals another honeycomb structure, in the upper-left part of the image, which can be attributed to the underlying silicon layer. In this structure, the distance between two adjacent hexagonal holes is around 0.44 nm. Describing the precise atomic arrangement of this underlying silicon lattice requires combining theoretical calculations with experimental data. Although it is hard to provide the precise atomic model with this FFT-based method, in the context, the FFT treatment can help us understand this intercalated silicon structure and confirm that it is a well ordered honeycomb arrangement.

To further examine the electronic properties of our intercalated sample, $\mathrm{d}I/\mathrm{d}V$ spectroscopy was performed locally on both graphene/Ir and graphene/Si/Ir areas. The measurements shown in Fig. 9 are averages, each calculated from a series of individual spectra obtained at the corresponding location. For graphene on Ir(111), our $\mathrm{d}I/\mathrm{d}V$ data show the existence of a local maximum around 0.3 eV below the Fermi level, as shown by the dashed-line arrow in Fig. 9(a). This maximum must be related to the Ir(111) surface state, for which a value of 0.4 eV has been reported.[36] This result reveals that the interaction between graphene and its underlying substrate is consistent with that found in the previous work, where it was reported that the graphene π band hybridizes strongly with the Ir 5d state near the Fermi level.[37] With silicon intercalation, this maximum feature is absent (the black spectra). This directly demonstrates that intercalated silicon effectively weakens the interaction between the graphene and the Ir substrate. More-

over, without silicon intercalation, we see that the spectrum is asymmetric. After silicon intercalation, the spectrum becomes symmetric. This symmetry resembles the intrinsic graphene. Therefore, our data reveals that silicon-intercalated graphene on Ir(111) behaves like the intrinsic graphene.

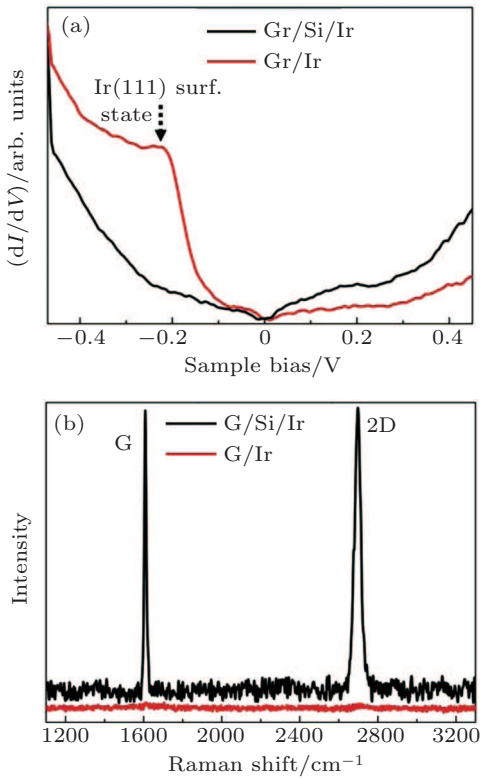

Fig. 9. (a) The $\mathrm{d}I/\mathrm{d}V$ spectroscopy measured on both the intercalated area (black line) and the un-intercalated area (red line) of the image shown in Fig. 2(a). The local maximum of the red spectrum around 0.3 eV is caused by the Ir surface state and is indicated by the dashed-line arrow. (b) Comparison of Raman spectra at 532 nm for graphene fabricated on Ir(111) before and after silicon intercalation, denoted as red and black lines, respectivley. After silicon-layer intercalation, the two prominent features of graphene, G and 2D peaks, are visible, and the D peak is absent.[27]

From the foregoing, we can conclude only that for a small area the quality of graphene after silicon intercalation is almost as good as the intrinsic graphene, so we also need to characterize the sample's physical properties from the macroscopic view. As Raman spectroscopy has been widely used in characterizing the properties of graphitic materials,[38,39] we employ it to characterize the physical properties of silicon-intercalated graphene on Ir(111). In order to compare un-intercalated graphene and silicon-intercalated graphene, we obtained Raman spectra of both systems from the samples of graphene/Ir and graphene/Si/Ir, as shown in Fig. 9(b). The graphene/Si/Ir sample was prepared by cycles of silicon deposition plus annealing till a large-scale Si-intercalated interface was produced between the graphene and the Ir substrate. Before intercalation, there is no Raman signal from the sample of graphene/Ir, indicated by the red line in Fig. 9(b), owing to the hybridization between the π bands of graphene and bulk Ir(111) substrate, which is in agreement with a previous study.[37] After silicon intercalation, the two prominent Raman features of graphene, the G peak and the 2D peak, emerge in the curve obtained from the graphene/Si/Ir sample. It is obvious that the silicon layer effectively decouples the interaction between graphene and the Ir(111) substrate. The blue shift of both the G peak and the 2D peak must be caused by a little mechanical strain and the charge from the underlying silicon.[40,41] In addition, the absence of the D peak in the curve indicates that the intercalated graphene has nearly no defects. Therefore, combining Raman spectra with the $\mathrm{d}I/\mathrm{d}V$ data discussed above, we conclude that the properties of the silicon-intercalated graphene on Ir(111) are almost the same as those of the freestanding monolayer graphene.

In this work, we derived the structure of the intercalated silicon layer from STM and LEED, and then investigated graphene's electronic properties by $\mathrm{d}I/\mathrm{d}V$ and Raman spectroscopy, showing that silicon intercalation effectively decouples the interaction between graphene and the Ir(111) substrate while keeping graphene's original high quality.

5. Conclusions and outlook

We reviewed the intercalation of metals or silicon at the interface of epitaxial graphene and its substrate. Seven kinds of metals, Pt, Pd, Ni, Co, Au, In, and Ce, have been successfully intercalated between graphene and the Ru(0001) substrate. For all these metals, the perfect atomic lattice of the graphene layer is preserved after intercalation. The diversity of the intercalated elements and corresponding structures prove that our convenient intercalation method is a universal approach for metals in graphene/Ru(0001) and also has a potential for tuning the transport properties of epitaxial graphene for future applications. This work also provides an efficient way to investigate the physics and the applications of underlying atomic layers and islands of metals with the protection of the stable graphene monolayer. With regard to silicon intercalation, we demonstrated that it is possible to intercalate Si layer at the interface of epitaxially grown, high quality graphene and its metal substrate (Ru(0001) or Ir(111)) and still maintain the graphene crystallinity and achieve electronic decoupling from the metal. Moreover, we have shown that it is possible to intercalate thicker layers of Si, allowing the atomic control of the distance between the graphene and the metal substrate. These results indicate the possibility of incorporating graphene-based structures with Si-based materials and can be very important for technological progress in materials science.

References

[1] Geim A K and Novoselov K S 2007 *Nat. Mater.* **6** 183

[2] Tombros N, Jozsa C, Popinciuc M, Jonkman H T and van Wees B J 2007 *Nature* **448** 571

[3] Novoselov K S, Jiang Z, Zhang Y, Morozov S V, Stormer H L, Zeitler U, Maan J C, Boebinger G S, Kim P and Geim A K 2007 *Science* **315** 1379

[4] Wang F, Zhang Y B, Tian C S, Girit C, Zettl A, Crommie M and Shen Y R 2008 *Science* **320** 206

[5] Li X S, Cai W W, An J H, Kim S, Nah J, Yang D X, Piner R, Velamakanni A, Jung I, Tutuc E, Banerjee S K, Colombo L and Ruoff R S 2009 *Science* **324** 1312

[6] Sutter P, Hybertsen M S, Sadowski J T and Sutter E 2009 *Nano Lett.* **9** 2654

[7] Pan Y, Shi D X and Gao H J 2007 *Chin. Phys.* **16** 3151

[8] Pan Y, Zhang H G, Shi D X, Sun J T, Du S X, Liu F and Gao H J 2009 *Adv. Mater.* **21** 2777

[9] Marchini S, Günther S and Wintterlin J 2007 *Phys. Rev. B* **76** 075429

[10] Sutter P W, Flege J I and Sutter E A 2008 *Nat. Mater.* **7** 406

[11] Vázquez de Parga A L, Calleja F, Borca B, Passeggi M C G, Hinarejos J J, Guinea F and Miranda R 2008 *Phys. Rev. Lett.* **100** 056807

[12] Dedkov Y S, Fonin M, Rudiger U and Laubschat C 2008 *Phys. Rev. Lett.* **100** 107602

[13] N'Diaye A T, Coraux J, Plasa T N, Busse C and Michely T 2008 *New J. Phys.* **10** 043033

[14] Gao L, Guest J R and Guisinger N P 2010 *Nano Lett.* **10** 3512

[15] Sutter P W, Albrecht P M and Sutter E A 2010 *Appl. Phys. Lett.* **97** 213101

[16] Shikin A M, Prudnikova G V, Adamchuk V K, Moresco F and Rieder K H 2000 *Phys. Rev. B* **62** 13202

[17] Varykhalov A, Sánchez-Barriga J, Shikin A M, Biswas C, Vescovo E, Rybkin A, Marchenko D and Rader O 2008 *Phys. Rev. Lett.* **101** 157601

[18] Enderlein C, Kim Y S, Bostwick A, Rotenberg E and Horn K 2010 *New J. Phys.* **12** 033014

[19] Farías D, Shikin A M, Rieder K H and Dedkov Y S 1999 *J. Phys.: Condens. Matter* **11** 8453

[20] Starodubov A G, Medvetski M A, Shikin A M and Adamchuk V K 2004 *Physics of the Solid State* **46** 1340

[21] Dedkov Y, Shikin A, Adamchuk V, Molodtsov S, Laubschat C, Bauer A and Kaindl G 2001 *Phys. Rev. B* **64** 035405

[22] Sutter P, Sadowski J T and Sutter E A 2010 *J. Am. Chem. Soc.* **132** 8175

[23] Zhang H, Fu Q, Cui Y, Tan D L and Bao X H 2009 *J. Phys. Chem. C* **113** 8296

[24] Premlal B, Cranney M, Vonau F, Aubel D, Casterman D, De Souza M M and Simon L 2009 *Appl. Phys. Lett.* **94** 263115

[25] Huang L, Pan Y, Pan L D, Gao M, Xu W Y, Que Y D, Zhou H T, Wang Y L, Du S X and Gao H J 2011 *Appl. Phys. Lett.* **99** 163107

[26] Mao J H, Huang L, Pan Y, Gao M, He J, Zhou H, Guo H, Tian Y, Zou Q, Zhang L, Zhang H, Wang Y, Du S, Zhou X, Neto A H C and Gao H J 2012 *Appl. Phys. Lett.* **100** 093101

[27] Meng L, Wu R, Zhou H, Li G, Zhang Y, Li L, Wang Y and Gao H J 2012 *Appl. Phys. Lett.* **100** 083101

[28] Sutter E, Acharya D P, Sadowski J T and Sutter P 2009 *Appl. Phys. Lett.* **94** 133101

[29] Corso M, Auwarter W, Muntwiler M, Tamai A, Greber T and Osterwalder J 2004 *Science* **303** 217

[30] Zhou S Y, Gweon G H, Fedorov A V, First P N, De Heer W A, Lee D H, Guinea F, Neto A H C and Lanzara A 2007 *Nat. Mater.* **6** 770

[31] Bostwick A, Ohta T, Seyller T, Horn K and Rotenberg E 2007 *Nat. Phys.* **3** 36

[32] Rutter G M, Crain J N, Guisinger N P, Li T, First P N and Stroscio J A 2007 *Science* **317** 219

[33] Peres N M R, Klironomos F D, Tsai S W, Santos J R, dos Santos J M B L and Neto A H C 2007 *Europhys. Lett.* **80** 67007

[34] Zhang Y, Brar V W, Wang F, Girit C, Yayon Y, Panlasigui M, Zettl A and Crommie M F 2008 *Nat. Phys.* **4** 627

[35] Hattab H, N'Diaye A T, Wall D, Jnawali G, Coraux J, Busse C, van Gastel R, Poelsema B, Michely T, Meyer zu Heringdorf F J and Horn-von Hoegen M 2011 *Appl. Phys. Lett.* **98** 141903

[36] Vanderveen J F, Himpsel F J and Eastman D E 1980 *Phys. Rev. B* **22** 4226

[37] Starodub E, Bostwick A, Moreschini L, Nie S, Gabaly F, McCarty K and Rotenberg E 2011 *Phys. Rev. B* **83** 125428

[38] Malard L M, Pimenta M A, Dresselhaus G and Dresselhaus M S 2009 *Phys. Rep.* **473** 51

[39] Ferrari A C, Meyer J C, Scardaci V, Casiraghi C, Lazzeri M, Mauri F, Piscanec S, Jiang D, Novoselov K S, Roth S and Geim A K 2006 *Phys. Rev. Lett.* **97** 187401

[40] Casiraghi C, Pisana S, Novoselov K S, Geim A K and Ferrari A C 2007 *Appl. Phys. Lett.* **91** 233108

[41] Rohrl J, Hundhausen M, Emtsev K V, Seyller T, Graupner R and Ley L 2008 *Appl. Phys. Lett.* **92** 201918